The Journal of Neuroscience, October 15, 2001, *21*(20):8072–8081

Long-Lasting Aberrant Tubulovesicular Membrane Inclusions Accumulate in Developing Motoneurons after a Sublethal Excitotoxic Insult: A Possible Model for Neuronal Pathology in Neurodegenerative Disease

Olga Tarabal[1], Jordi Calderó[1], Jerònia Lladó[1], Ronald W. Oppenheim[2], and Josep E. Esquerda[1]

[1]*Unitat de Neurobiologia Cellular, Departament de Ciències Mèdiques Bàsiques, Facultat de Medicina, Universitat de Lleida, E25198 Lleida, Catalonia, Spain, and* [2]*Department of Neurobiology and Anatomy and Neuroscience Program, Wake Forest University School of Medicine, Winston-Salem, North Carolina 27157*

We have previously shown that chronic treatment of chick embryos [from embryonic day 5 (E5) to E9] with NMDA rescues spinal cord motoneurons (MNs) from programmed cell death. In this situation, MNs exhibit a reduced vulnerability to acute excitotoxic lesions and downregulate NMDA and AMPA–kainate receptors. Here, we report that this treatment results in long-lasting sublethal structural changes in MNs. In Nissl-stained sections from the spinal cord of NMDA-treated embryos, MNs display an area adjacent to an eccentrically positioned nucleus in which basophilia is excluded. Ultrastructurally, MNs accumulate tubulovesicular structures surrounded by Golgi stacks. Thiamine pyrophosphatase but not acid phosphatase was detected inside the tubulovesicular structures, which are resistant to disruption by brefeldin A or monensin. Immunocytochemistry reveals changes in the content and distribution of calcitonin gene-related peptide, the KDEL receptor, the early endosomal marker EEA1, and the recycling endosome marker Rab11, indicating that a dysfunction in membrane trafficking and protein sorting occurs in these MNs. FM1-43, a marker of the endocytic pathway, strongly accumulates in MNs from isolated spinal cords after chronic NMDA treatment. Changes in the distribution of cystatin C and presenilin-1 and an accumulation of amyloid precursor protein and β-amyloid product were also observed in NMDA-treated MNs. None of these alterations involve an interruption of MN-target (muscle) connections, as detected by the retrograde tracing of MNs with cholera toxin B subunit. These results demonstrate that chronic NMDA treatment induces severe changes in the motoneuronal endomembrane system that may be related to some neuropathological alterations described in human MN disease.

Key words: ALS; autophagy; chick embryo; Golgi apparatus; glutamate receptor-mediated excitotoxicity; membrane traffic; motoneuron

Glutamate receptors present in spinal cord motoneurons (MNs) are involved in several forms of acute and chronic neurodegeneration. Acute glutamate-mediated excitotoxic neuronal death is a relevant pathogenetic mechanism in spinal cord lesions developed after ischemia or trauma. These lesions can be experimentally simulated by the acute administration of excitotoxins acting on glutamate receptors (Wrathall et al., 1994; Agrawal and Fehlings, 1997). By contrast, in chronic neurodegenerative diseases involving glutamate toxicity, such as sporadic amyotrophic lateral sclerosis (ALS), the loss of MNs is gradual and progressive. The microscopic pathology of MNs in ALS shows various degrees of degenerative changes, including several types of cytoplasmic inclusions, chromatolysis, and axonopathy with axonal spheroids (Chou, 1995). Although the cellular pathway responsible for the neuronal loss in ALS remains undefined, it appears that it is not apoptotic in nature (Migheli et al., 1999). In addition to these well recognized pathological alterations, more subtle changes in subcellular organelles have been described in altered MNs from human and experimental ALS. These changes consist of a disorganization and fragmentation of Golgi apparatus that, as suggested, may affect the transport, processing, and targeting of proteins in the secretory pathways, causing a neuronal dysfunction that may be relevant in ALS pathogenesis (Gonatas et al., 1992; Mourelatos et al., 1996).

The excitotoxic hypothesis of ALS is based primarily on data showing that many patients with sporadic ALS displayed a selective loss of glutamate transport. This creates a defect in the clearance of extracellular glutamate leading to its chronic elevation that is toxic to MNs (Rothstein, 1996). In contrast to the acute excitotoxic neuronal death that is caused by a rapid and severe ionic imbalance of the intracellular milieu, the mechanisms triggered by glutamate to induce a slow neurodegeneration similar to that found in ALS are not known. Furthermore, a link between slowly developing glutamate neurotoxicity and ALS-related organelle pathology remains to be experimentally demonstrated.

In the present study, we report a new paradigm of glutamate receptor-mediated neurotoxicity in chick embryo spinal cord, in which injured MNs, instead of suffering a rapid cell death, develop long-lasting changes involving the endomembrane system. These alterations comprise the redistribution of Golgi apparatus and the formation of an intricate network of tubulovesicular structures that evolve to cytoplasmic autophagosome-like inclusions. Because most of these changes resemble those seen in MN

Received April 23, 2001; revised June 28, 2001; accepted July 17, 2001.

This work was supported by grants from the Ministerio de Educación y Ciencia (SAF200-0168), Fundació La Marató de TV3, Fundació La Caixa, Ajuntament de Lleida, and National Institutes of Health Grant NS20402 (R.W.O.). We thank Ester Vàzquez and Carme Guerris for their technical assistance.

Correspondence should be addressed to Josep E. Esquerda, Unitat de Neurobiologia Cellular, Departament de Ciències Mèdiques Bàsiques, Facultat de Medicina, Universitat de Lleida, Rovira Roure 44, E25198 Lleida, Catalonia, Spain. E-mail: Josep.Esquerda@cmb.udl.es.

diseases, the model reported here may be useful to gain new insights into the relationship between glutamate excitotoxicity and chronic motoneuronal degeneration in sporadic ALS.

MATERIALS AND METHODS

Embryos and pharmacological experiments. Fertilized chicken eggs purchased from COPAGA (Lleida, Catalonia, Spain) were incubated in the laboratory. Embryos from embryonic day 5 (E5) to E9 were treated daily with NMDA (Sigma, St. Louis, MO). This drug was dissolved in saline and dropped in volumes of 50–100 μl onto the chorioallantoic membrane through a window in the shell. Doses of NMDA were: 0.5 mg on E5 and E6 and 0.25 mg daily on E7, E8, and E9. Embryos injected with identical volumes of physiological saline were used as controls. At time of killing, embryos were staged according to Hamburger and Hamilton (1951) stage series.

Cell counts were performed on serial paraffin sections stained with thionin as described previously (Calderó et al., 1997). Some sections were also processed for Palmagrem's neurofibrilar silver stain.

Isolated spinal cord experiments. Spinal cords from E10 embryos previously treated *in ovo* with either saline or NMDA were rapidly dissected and placed in ice-cold low-sodium buffer containing (in mM): 139 sucrose, 57.5 NaCl, 5 KCl, 2 $MgCl_2$, 2 $CaCl_2$, 12 glucose, and 10 HEPES, pH 7.4. Spinal cords were then placed on a tissue slice chamber (Fine Science Tools, Heidelberg, Germany) and continuously oxygenated and perfused with the abovementioned buffer for 45 min at 20°C. Samples were then incubated for 60 min with 5 μg/ml of brefeldin A (Sigma), 10 μM monensin, or saline dissolved in normal sodium buffer containing (in mM): 124 NaCl, 5 KCl, 2 $MgCl_2$, 2 $CaCl_2$, 20 glucose, 1.25 KH_2PO_4, and 3–5 $NaCHO_3$, pH 7.4, and bubbled with 95% O_2 and 5% CO_2. Samples were fixed by immersion with 2.5% glutaraldehyde in 0.1 M phosphate buffer (PB), pH 7.4, for 2 hr at 4°C. Lumbar spinal cords were then processed for electron microscopy according to standard procedures.

Similar experiments were done for studies on endocytosis in spinal cords from E16 embryos. Samples were incubated in the perfusion chamber with 5 μM FM1-43 (Molecular Probes, Eugene, OR) for 3 hr. Samples were then fixed with 4% paraformaldehyde in 0.1 M PB, pH 7.4, sectioned transversally with a vibratome, and imaged by a Zeiss (Oberkochen, Germany) LSM-310 confocal microscope using the 488 nm argon ion laser excitation source.

Retrograde tracing of MNs. One mg of lyophilized cholera toxin B subunit (CTB; List Biological Laboratories, Campbell, CA) was reconstituted with 1 ml of distilled water, dialyzed against PB to remove NaN_3, and concentrated to 1% with a Centricon-10 microconcentrator (Amicon, Beverly, MA). Retrograde tracing of MNs was performed by applying 5 μl of CTB distributed in three intramuscular injections into the right hindlimb of NMDA-treated embryos *in ovo*, by means of pulled glass capillary tubes attached to a 10 μl Hamilton syringe. Embryos were killed 5, 10, 15, or 20 hr later.

Electron microscopy and enzyme cytochemistry. Spinal cord samples from E6 to E21 embryos were fixed by immersion with 2.5% glutaraldehyde in 0.1 M PB, pH 7.4. After washing in PB, samples were post-fixed in 1% osmium tetroxide solution for 2 hr, dehydrated, and embedded in EMbed 812 (Electron Microscopy Sciences, Fort Washington, PA). Ultrathin sections were obtained from selected ventral horn areas of the lumbosacral enlargement, collected on copper grids, counterstained with uranyl acetate and lead citrate, and observed with a Zeiss EM 910 electron microscope.

For thiamine pyrophosphatase (TPPase) and acid phosphatase (APase) cytochemistry, samples were fixed for 4 hr at 4°C with 0.5% glutaraldehyde, 3% paraformaldehyde, and 5% sucrose in 0.1 M cacodylate buffer, pH 7.4. After washing, spinal cords were embedded in 2.5% agar in PB, cut by using a vibratome to obtain 50 μm transverse sections, and processed as described by Lewis (1977). Briefly, for TPPase, sections were incubated for 30 min to 2 hr at room temperature in a solution containing (in mM): 4 $Pb(NO_3)_2$, 5 $MnCl_2$, 80 Tris-maleate, pH 7.2, and 2.5 cocarboxylase and distilled water. For APase, sections were incubated for 10 min to 1 hr at room temperature in a solution containing (in mM): 40 Tris-maleate buffer, pH 5.2, 8 sodium β-glycerophospate, and 2.4 lead citrate and distilled water. Afterward, sections were washed, post-fixed in 1% osmium tetroxide solution embedded in EMbed 812 (Electron Microscopy Sciences), and then processed for electron microscopy.

Immunocytochemistry. Embryos were fixed with 4% paraformaldehyde in 0.1 M PB, pH 7.4, overnight at 4°C. After cryoprotection with 30% sucrose in 0.1 M PB, samples were frozen, and transverse sections (18 μm) from lumbar spinal cord were obtained. Sections were washed in PBS and 0.1% Triton X-100 and incubated with either 3% normal goat serum or 3% normal horse serum in PBS for 30 min. Double immunolabeling was performed in sections that were incubated overnight at 4°C with a mix of two primary antibodies diluted in PBS and 0.1% Triton X-100. The following antibodies were used: rabbit anti-rat calcitonin gene-related peptide (CGRP; 1:1000) from Peninsula Laboratories (San Carlos, CA); mouse anti-rat CGRP (1:1000) from RBI (Natick, MA); mouse anti-KDEL receptor (1:50), mouse anti-GS28 (1:50) from StressGen Biotechnologies (Victoria, Canada); goat anti-human presenilin-1 (PS1; 1:300), rabbit anti-β amyloid (1:100), rabbit anti-β amyloid precursor (1:100) from Serotec (Oxford, UK); rabbit anti-human cystatin C (1:500) from Dako (Glostrup, Denmark); mouse anti-ubiquitin (1:500), mouse anti-phosphorylated neurofilament-M and H (1:500) from Chemicon (Temecula, CA); goat anti-cholera toxin (1:4000) from List Biological Laboratories (Campbell, CA); and mouse anti-EEA1 (1:200) and mouse anti-Rab11 (1:200) from Transduction laboratories (Lexington, KY). After several washes in PBS, sections were incubated for 1 hr at room temperature with the appropriate mix of the following secondary antibodies from Molecular Probes: Alexa Fluor 488 goat anti-rabbit IgG (1:500), Alexa Fluor 488 goat anti-mouse IgG (1:1000), Alexa Fluor 488 goat anti-rabbit IgG (1:1000), and Alexa Fluor 488 monkey anti-goat IgG (1:1000). In some cases, sections were incubated with biotinylated secondary antibodies followed by the ABC immunoperoxidase procedure (Vector Laboratories, Burlingame, CA).

A specific squash procedure for specimen preparation adapted from Pena et al. (2001) was used in the case of EEA1 and Rab11 immunocytochemistry. Spinal cords were fixed with 4% paraformaldehyde in 0.1 M PB for 2–4 hr at 4°C and sectioned with a vibratome (300 μm of thickness). Individual sections were washed in PB and placed on SuperfrostPlus microscope slides (Menzel-Glaser, Germany), and a coverslip was applied to the tissue and squashed with a forceps. Preparations were then frozen in liquid N_2, and, after removing the coverslip, slides with the retained tissue were fixed in methanol at −20°C for 10 min. After PBS washing, immunocytochemistry was performed as described above.

Some squash preparations were incubated with the lectin wheat germ agglutinin (WGA) labeled with Alexa Fluor 488 (5 μg/ml; Molecular Probes) to label Golgi apparatus. This lectin was not used systematically as a Golgi marker in tissue sections because, in our hands, it shows a high background staining on chick MNs.

Some sections were counterstained with 3 mM 4′,6-diamidino-2-phenylindole dihydrochloride (DAPI; 50 ng/ml; Molecular Probes) for 5 min at room temperature to visualize chromatin morphology.

Immunofluorescent preparations were mounted with Vectashield (Vector Laboratories) or with a laboratory-made anti-fading mounting medium (0.1 M Tris-HCl buffer, pH 8.5, 20% glycerol, 10% Moviol, and 0.1%, 1,4-diazabicyclo [2.2.2] octane). Images were obtained using a cooled CCD camera Ultrapix SK 1600 (Life Science Resources, Cambridge, UK) attached to a Nikon Eclipse E600 microscope equipped with epifluorescence illumination and the appropriate selective filters, and processed using the Esprit software (Life Sciences Resources). Alternatively, a confocal laser-scanning Zeiss LSM-310 microscope equipped with 543 mm helion–neon and 488 nm argon–ion lasers was used.

RESULTS

A single injection of NMDA in chick embryos older than E7 induces an acute and massive excitotoxic necrosis in spinal cord MNs (Calderó et al., 1997). By contrast, chronic treatment with NMDA, starting before this stage of vulnerability to excitotoxic necrosis has been developed (i.e., on E5 or E6), induces protection of spinal cord neurons from cell death induced by excitotoxins acting on NMDA and non-NMDA glutamate receptors. Moreover, chronic NMDA treatment administered during the period of naturally occurring programmed cell death (PCD) of MNs (E5–E9), is also able to partially rescue MNs from normal PCD (Fig. 1). These results are in agreement with our previous report in which, in addition, we have shown that the NR1 subunit of NMDA receptor was downregulated concomitant with protection from excitotoxic necrosis (Lladó et al., 1999).

Although chronic NMDA treatment prevents the acute destruction of MNs that would otherwise occur as a consequence of

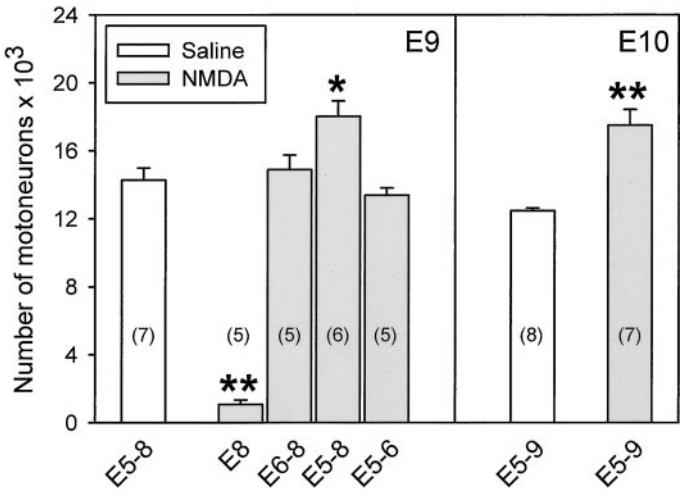

Figure 1. Changes in MN numbers (mean ± SEM) in the lumbar lateral motor column of E9 and E10 chick embryos after treatment with either saline or different regimens of NMDA. NMDA was administered on E8 only, daily from E6 to E8, daily from E5 to E8, or on E5 and E6 (in the case of embryos killed on E9); and daily from E5 to E9 (in the case of embryos killed on E10). Doses of NMDA were 0.5 mg on E5 and E6 and 0.25 mg on E7, E8, and E9. *Numbers* in *parentheses* indicate sample sizes. $^{*}p < 0.01$, $^{**}p < 0.001$ versus saline (Student's *t* test).

a single NMDA pulse on E7, it does not prevent the development of more subtle and persistent cytopathological changes. These involve disturbances in membrane trafficking and other pathological alterations in intracellular organelles that had been suggested before (Calderó et al., 1997) and are now confirmed and described here in detail.

Chronic NMDA treatment induces vacuolization and tubulation of intracellular membrane compartments

By beginning chronic NMDA treatment on E5, only a few MNs die by acute excitotoxic necrosis on E5 or E6. The remaining MNs did not show any apparent alterations in Nissl-stained samples from E5 to E10 embryos. However, when MNs were observed in the electron microscope, striking alterations were observed mainly affecting the endomembrane system. These alterations were seen in an increasing number of MNs from E8 to E10. Altered MNs had a large number of vacuoles presumably arising from the endoplasmic reticulum (ER), some of which were interconnected with small tubules filled with dense material. Often, the tubules appeared concentrated in a region adjacent to the nucleus and surrounded by Golgi profiles (Fig. 2*A*,*B*). TPPase cytochemistry was used as a marker for the *trans*-Golgi region (Novikoff and Goldfischer, 1961). TPPase positivity was seen, as expected, in the most external stacks of Golgi apparatus and in NMDA-induced tubulovesicular structures (Fig. 2*C*). Tubulovesicular structures were devoid of APase activity (data not shown). The ultrastructural organization of nuclear chromatin in these MNs appeared essentially normal.

From these results it is evident that chronic NMDA treatment induces hypertrophy of a specific intracellular membrane compartment of unknown origin. The following experiments were done to gain further information about the properties of this compartment.

Brefeldin A is a widely used agent in membrane trafficking studies that has profound effects on the secretory pathway, inducing structural changes in intracellular membrane compartments (Klausner et al., 1992). Brefeldin A causes the intermixing of Golgi components with the ER and induces membrane tubulation and fusion of endosomes, lysosomes, and the *trans*-Golgi network (Lippincott-Schwartz et al., 1991). To explore how brefeldin A affects the organization of intracellular membrane compartments altered by NMDA treatment, spinal cords from E10 embryos previously treated with either saline or NMDA (E5–E9) were isolated and perfused with modified oxygenated Tyrode's solution (see Materials and Methods), and incubated in the presence or absence of brefeldin A. The ultrastructural analysis of MNs showed that, after 1 hr of incubation in brefeldin A, the Golgi apparatus became completely disorganized in both normal or NMDA-treated embryos. Other features indicating that brefeldin A was effective in isolated spinal cords were the induction of the so-called "BFA bodies" (Orci et al., 1993) and membrane tubulation in MNs from control embryos (data not shown). However, NMDA-induced tubular structures along with their dense contents were unaltered after brefeldin A treatment (Fig. 3*A*). Furthermore, the Na^+ ionophore monensin, another drug that affects the secretory pathway, was applied in the same way as brefeldin A in isolated spinal cord. Ultrastructural morphology revealed that monensin produced the typical changes in MNs previously described in non-neural cells (Ledger and Tanzer, 1984). These changes consist of the disruption of Golgi stacks that were replaced by vacuoles with smooth membranes and the densification of mitochondrial matrix. However, monensin did not affect NMDA-induced membrane tubules (Fig. 3*B*).

Persistence of NMDA-induced redistribution of Golgi and endoplasmic reticulum in motoneurons

The rearrangement of intracellular membrane compartments involving Golgi apparatus and ER induced by NMDA in MNs persisted long after stopping the treatment. These remarkable cytopathological changes were detectable in more mature MNs even by light microscopy. In Nissl-stained sections from NMDA-treated (E5–E9) embryos older than E14, most of the surviving MNs displayed an area adjacent to the nucleus in which basophilia was excluded, indicating that a displacement of the rough ER to the cellular margin had occurred. At the same time, the nucleus occupied a clearly eccentric position (Fig. 4*A*,*A′*). A high proportion of surviving MNs showed this Nissl-excluded region (NER) as a consequence of NMDA treatment (36 ± 3.39%; mean ± SEM).

To explore how the relocation of ER affects the placement of other intracellular membrane compartments, we first looked for changes in Golgi apparatus. Because most intrinsic Golgi markers do not work in avian tissues, we applied CGRP immunostaining to trace Golgi areas. This is based on our observation that, in rat MNs, CGRP accumulates in *trans*-Golgi stacks and secretory vesicles (Calderó et al., 1992). Similar results were obtained in E16 chick embryo MNs (data not shown). Moreover, we have recently found a close colocalization between CGRP and the Golgi-soluble *N*-ethylmaleimide-sensitive factor attachment protein receptor GS-28 (Subramaniam et al., 1996) and CGRP and the Golgi marker WGA (Fig. 4*F*). CGRP immunostaining in normal MNs displayed a fine punctuate pattern distributed around the nucleus and scattered in the entire MN cell body (Fig. 4*B*). By contrast, in NMDA-treated MNs, the location of CGRP was altered, being redistributed in a circle that surrounded an area corresponding to the above mentioned juxtanuclear NER (Fig. 4*B′*). We further examined how other membrane compartments that are structurally and functionally related to Golgi were affected by NMDA. The KDEL receptor (KDELr) is associated

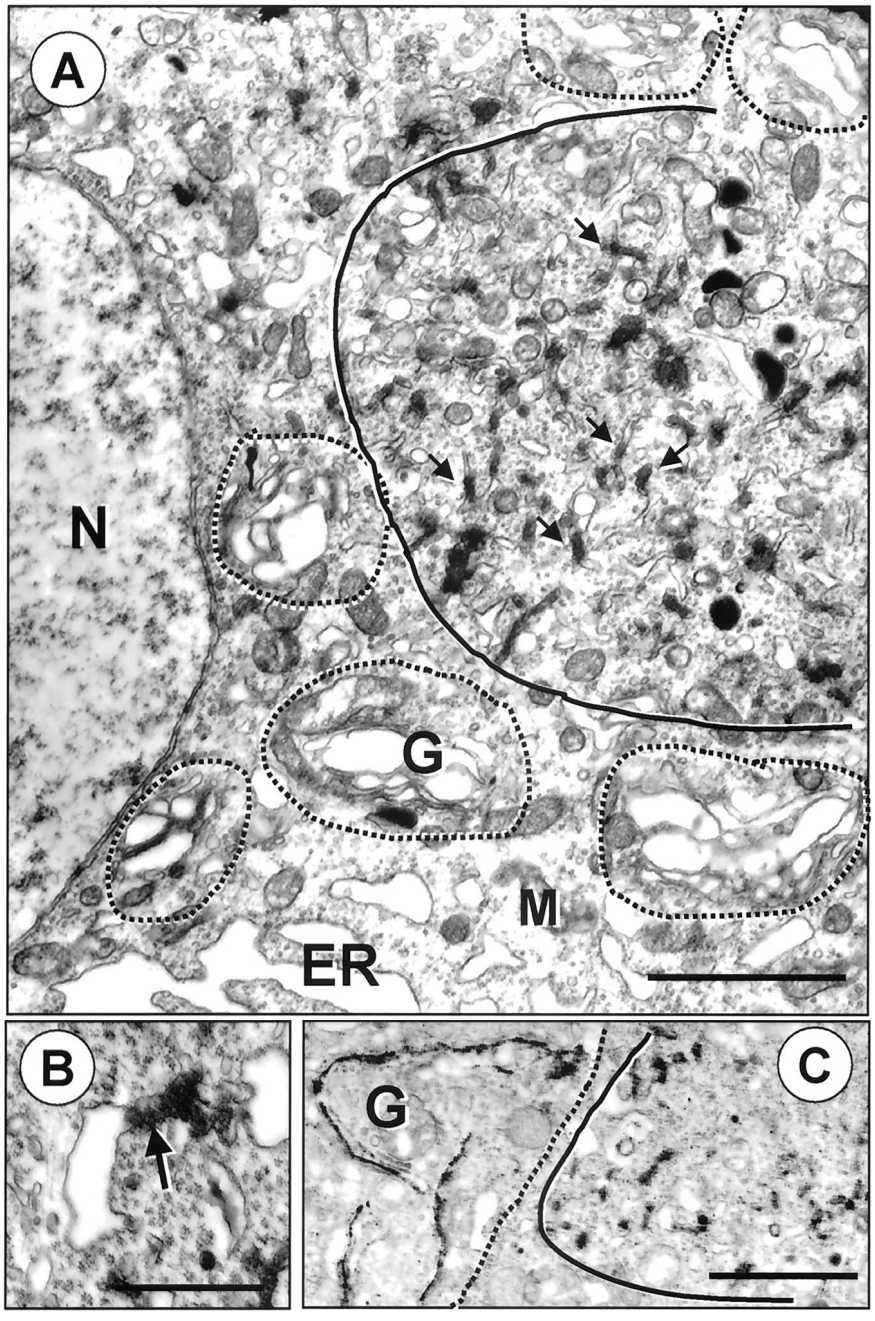

Figure 2. Ultrastructural micrographs from MNs of E10 NMDA-treated embryos. *A* shows that the core of the Nissl-excluded region (marked with a *continuous line*) is formed by an interconnected network of membrane-bounded tubules (*arrows*) and vesicles, some of them filled with an electrodense material; this complex is peripherally surrounded by Golgi stacks (*dashed lines*) and is located in a juxtanuclear area of the MN; endoplasmic reticulum (*ER*), which is mainly located outside of this region, at the periphery of cell body, displays a dilated profile. *B* shows a high magnification of tubulovesicular structures partially filled with electrodense material (*arrow*). *C,* TPPase cytochemistry displays a positive reaction in NMDA-induced tubulovesicular structures (delimitated by a *continuous line*) and in the most external stacks of Golgi apparatus (*G*, delimitated by a *dashed line*). *N,* Nucleus; *M,* mitochondrion. Scale bars: *A*, 2.30 μm; *B*, 1.15 μm; *C*, 1.80 μm.

with specific intracellular membrane domains corresponding to the ER–Golgi intermediate compartment (ERGIC), and it is involved in retrograde transport of vesicles from Golgi to ER. In these compartments, KDEL-tagged resident ER proteins are retrieved before entering the Golgi apparatus and the secretory pathway (Lewis and Pelham, 1992; Griffiths et al., 1994). As expected, in normal E16 MNs KDELr was present in structures surrounding CGRP-immunopositive Golgi areas (Fig. 4*C*,*C′*). After chronic NMDA treatment, however, the redistribution of CGRP-positive Golgi stacks was associated with a new location of the KDELr-positive ERGIC compartment, which was shifted out of the Golgi (Fig. 4*D,D′*). The peripheral position of KDELr encircling Golgi areas signals a *cis–trans* polarity at the edge of the NER from periphery to center. This suggests that the core of the NER belongs to *trans*-Golgi. In this region, secretory and endocytic pathways converge forming the *trans*-Golgi network (TGN), an intricate system of tubulovesicular membranes that is the main site for sorting transport and secretory vesicles (Mellman and Simons, 1992) and for targeting synaptic membrane receptors in dendrites (Trimmer, 1999). The most common marker for delimiting TGN is TGN38 but, unfortunately, it cannot be applied for this purpose in avian cells. In spite of the absence of positive data regarding accumulation of TGN membrane markers in NER, we detected an accumulation of presumptive post-Golgi vesicles containing cystatin C inside NER (Fig. 4*E′*). Conversely, in normal MNs, cystatin C vesicles were homogeneously distributed in the cell body matching the normal broad location of Golgi (Fig. 4*E*). Moreover, other post-Golgi vesicles containing products of the secretory pathway, such as granules containing CGRP and glycoproteins labeled with WGA (Fig. 4*F*), were also concentrated inside the NER. Proteins known to be processed along the secretory pathway were also

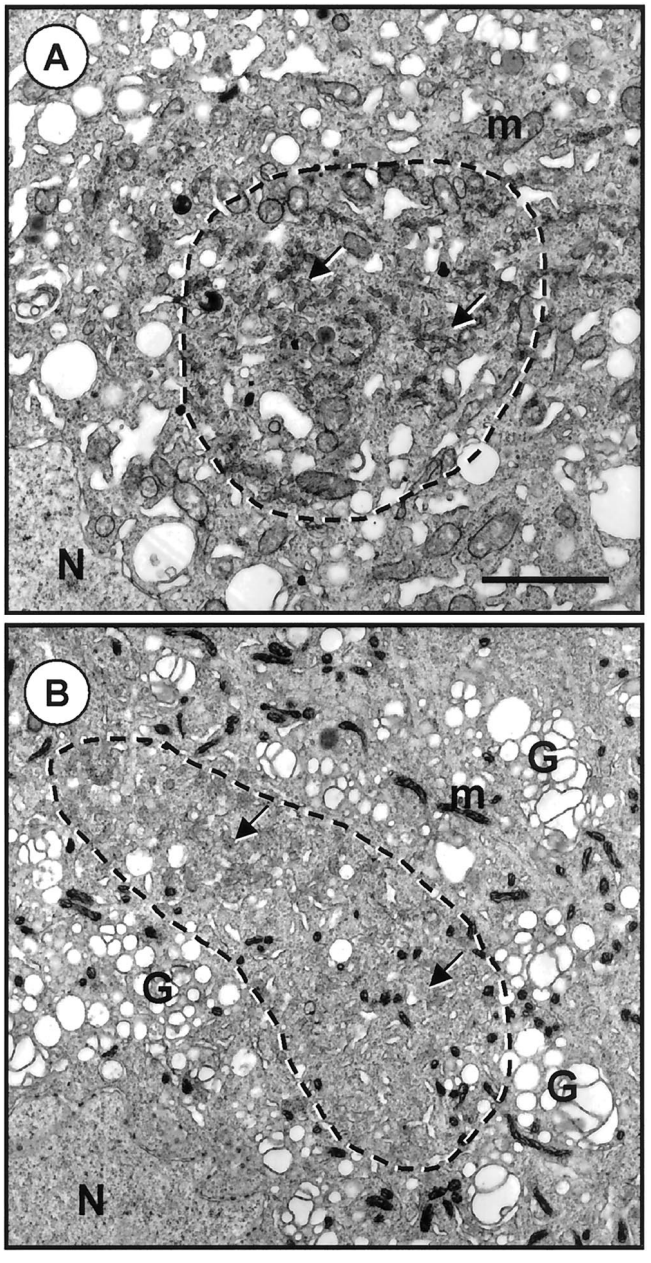

Figure 3. Ultrastructural changes in MNs from NMDA-treated embryos induced by brefeldin A (*A*) or monensin (*B*). *A,* brefeldin A induces a profound disorganization of Golgi apparatus, which disappears at the boundary of Nissl-excluded region (*dashed lines*); tubulovesicular structures (*arrows*) remain unaltered. *B*, Monesin treatment induces an alteration of Golgi apparatus (*G*) that is transformed to smooth membraned vacuoles; no changes are seen in tubulovesicular structures (*arrows*) inside the Nissl-excluded region (*dashed lines*). *m,* Mitochondria; *N,* nucleus. Scale bar (in *A*): *A*, 2.30 μm; *B*, 2.90 μm.

found to accumulate inside NER. This was the case for amyloid precursor protein (APP) and its processed product fragment β-amyloid peptide (βAP). In normal MNs, the expression level of neither of these products was high enough to be detectable by immunocytochemistry. However, in NMDA-treated E16 MNs an immunopositive signal was detected inside the NER, indicating that both APP and βAP had been accumulated in this region (Fig. 4*G*,*H*).

In addition to the reorganization of the endomembrane system, a change in the arrangement of the cytoskeleton was also indicated. Using antibodies against neurofilament proteins tubulin or phalloidin to trace actin filaments, we were not able to detect an accumulation of cytoskeletal proteins in MNs (data not shown). However, more subtle changes in cytoskeletal organization exist because, by using either antibodies that recognize phosphorylated neurofilaments or by silver staining, we observed a rearrangement of neurofibrils around NER (Fig. 5*A–C*).

To look for changes in the endocytic pathway membrane compartments after NMDA treatment, we performed immunocytochemical studies to detect the early endosomal marker EEA1 and the recycling endosome marker Rab11. The EEA1 antibody labeled many punctuate structures extensively distributed in normal MN cell bodies, being more prominent and expanded through the dendritic shaft. However, there was no evidence of accumulation of this marker inside NER in NMDA-treated embryos (data not shown). By contrast, Rab11 was moderately increased inside NER (Fig. 4*I*). The endocytic pathway was also functionally labeled by the incubation of isolated spinal cords from NMDA-treated embryos with FM1-43, which resulted in a marked accumulation of fluorescent granules in NER (Fig. 4*K*). It is known that, after long incubations, FM1-43 accumulates in TGN and late endosomes (Maletic-Savatic and Malinow, 1998).

All of the immunocytochemical data concerning NER are summarized in Table 1.

NMDA-induced changes in the organization of the Golgi and endoplasmic reticulum membranes do not involve the interruption of MN-target (muscle) connections

The cytological transformation of MNs observed after NMDA treatment is similar, in some aspects, to the changes observed during the cell body retrograde reaction after axotomy or chromatolysis (Barron et al., 1971; Lieberman, 1971). Although there is no evidence of severe axonal pathology in our protocol of NMDA treatment, we have examined whether the organelle pathology seen after NMDA treatment is distinct from the classical chromatolytic axonal reaction. First we compared the morphology of Nissl bodies in axotomized and in NMDA-treated MNs. In axotomized MNs, Nissl bodies break up and become dispersed in the form of dustlike basophilic particles with a clearly different pattern from that seen in NMDA-treated MNs (data not shown). Furthermore, to our knowledge, the ultrastructural pathology of axotomized neurons does not include the specific alterations we describe here. MNs displaying the typical organelle pathology after NMDA treatment were in fact connected with their target muscle because they could be retrogradely labeled with muscle-injected CTB. Anterograde axonal transport also appeared not to be affected, because CGRP was found in intramuscular nerves close to neuromuscular synapses. Finally, intramuscular nerves in NMDA-treated embryos were able to differentiate normal neuromuscular synapses that concentrated acetylcholine receptors (data not shown).

Retrograde tracing with CTB also allowed us to follow the fate of endocytic organelles carrying this toxin. We found that endocyted CTB is targeted in the cell bodies to Golgi and endolysosomal vesicles, similar to non-neural cells (Nambiar et al., 1993; Majoul et al., 1996). Double-labeling experiments in which the uptake of CTB was visualized in combination with CGRP showed that the former was never concentrated in the core of NER (Fig. 4*J*).

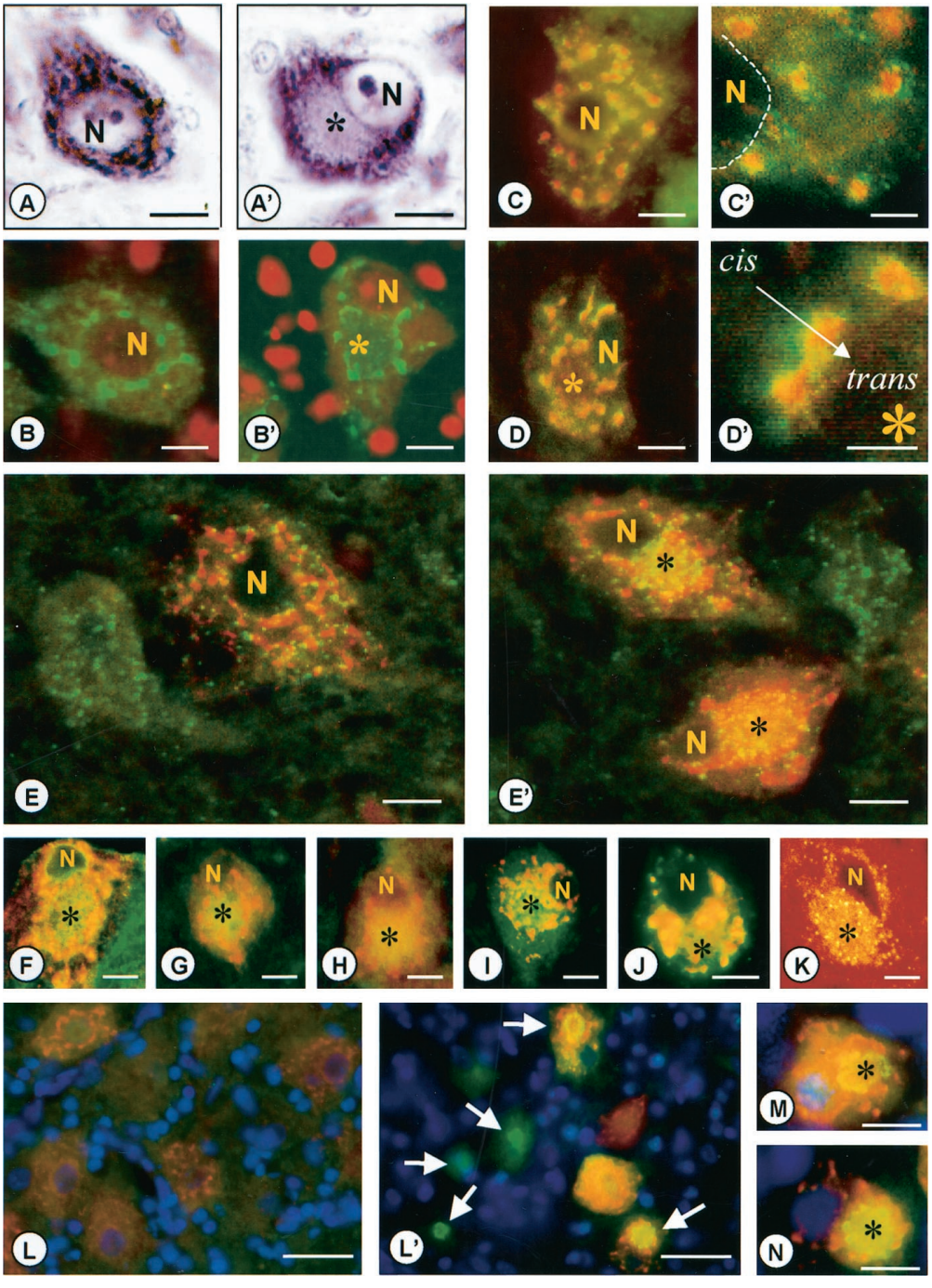

Figure 4. Morphological and immunocytochemical characterization of Nissl-excluded region in E16 MNs. *A, A′,* Thionin-stained paraffin sections to demonstrate that, after chronic NMDA treatment, MNs display an area adjacent to the nucleus in which basophilia or Nissl substance is excluded (*asterisk* in *A′*); compare *A′* with the normal pattern of Nissl staining in MNs of saline-treated embryos (*A*). *B, B′*, The CGRP immunostaining (*green*) in normal MNs shows a fine dotted pattern distributed in the entire MN cell body (*B*), which corresponds to Golgi stacks and secretory vesicles; conversely, in MNs from NMDA-treated embryos, CGRP immunolabeling shows a redistribution, forming a *circle* that surrounds the juxtanuclear Nissl-excluded region (*asterisk* in *B′*); the sections were counterstained with propidium iodide (*red*). *C–D′,* Double fluorescent immunolabeling to demonstrate the distribution of KDELr (*green*) and CGRP (*red*); *C* shows that, in normal MNs, KDELr is located in structures surrounding CGRP-immunopositive Golgi stacks; *C′* is a digital enlargement of *C*; in NMDA-treated embryos the redistribution of CGRP-positive Golgi stacks involves a relocation of the KDELr-positive ERGIC compartment out of the CGRP-immunopositive circle (*D*); *D′* is a digital enlargement of *D,* where the *cis–trans* polarization of Golgi apparatus, deduced from the KDELr location, is indicated with an *arrow*. *E, E′,* Double fluorescent immunolabeling for cystatin C (*green*) and CGRP (*red*); cystatin C-immunopositive granules are homogeneously distributed in the cytoplasm of normal MNs (*E*); by contrast, in NMDA-treated embryos, cystatin C granules are concentrated inside the Nissl-excluded region (*asterisk* in *E′*) surrounded by a CGRP-positive boundary. *F–I,* Sections from spinal cord of chronically treated NMDA embryos labeled with CGRP antibody (*red*), and WGA (*green* in *F*), or antibodies against APP (*green* in *G*), βAP (*green* in *H*), and Rab11 (a recycling endosome marker, *green* in *I*); all of these markers accumulate inside the Nissl-excluded region (*asterisk*), which is delimitated by CGRP immunostaining. *J* is from the spinal cord of an NMDA-treated embryo in which MNs were retrogradely labeled with muscle-injected CTB; the section was double-immunolabeled to demonstrate CGRP (*red*) and CTB (*green*). Note that CTB colocalizes in part with CGRP but does not accumulate inside the Nissl-excluded area (*asterisk*). *K* is a section from an isolated spinal cord of an NMDA-treated embryo incubated with FM1-43 showing the accumulation of this endocytic tracer inside the Nissl-excluded region (*). *L–N,* Triple fluorescent labeling to demonstrate CGRP (*red*), PS1 (*green*), and DNA (DAPI staining, *blue*). In normal MNs, PS1 immunoreactivity is not detectable (*L*); however, after NMDA treatment, PS1 immunoreactivity is markedly increased inside the Nissl-excluded region (*arrows* in *L′*). PS1 immunoreactivity exhibits a positive ring inside the Nissl-excluded region shown in *M* and *N* (*asterisk*). *N,* Nucleus. Scale bars: *A–B′, C, D–H, J, K,* 10 μm; *C′,* 5 μm; *D′,* 3 μm; *I,* 15 μm; *L,* 30 μm; *L′,* 35 μm; *M, N,* 20 μm.

Changes in presenilin-like immunoreactivity in motoneurons after NMDA treatment

Mutations in genes encoding presenilins 1 (PS1) and 2 (PS2) are involved in early-onset familial Alzheimer disease. In normal cells, PS1 and PS2 are located in intracellular membranous compartments, including the ER, Golgi complex, transitional compartments, and transport vesicles (Lah et al., 1997). However, the identity and molecular components of the subcompartments in which PSs reside have not been fully defined (Kim et al., 2000). Because NMDA treatment induces profound changes in the intracellular membrane compartmentation, we explored whether PS1-containing membrane domains were altered in neurons displaying NER. In normal MNs, PS1-like immunostaining was below the level of detection (Fig. 4*L*). By contrast, after NMDA treatment, PS1 immunoreactivity was markedly increased in a specific region inside NER on E16. MNs showed a central ring of

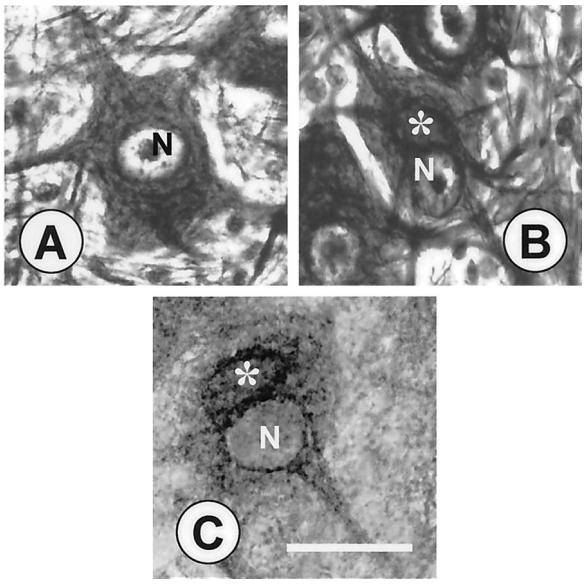

Figure 5. Neurofibrilar staining by means of silver impregnation (*A, B*) reveals a reorganization of cytoskeleton around NER in MNs of NMDA-treated embryos. Compare the MN from an E19 saline-treated embryo (*A*) with that from an E19 NMDA-treated embryo (*B*). A similar result is obtained after immunostaining of phosphorylated neurofilament proteins (*C*). *N,* Nucleus; * indicates the core of NER. Scale bar, 25 μm.

PS1 immunoreactivity inside NER surrounded by redistributed Golgi stacks immunostained with CGRP (Fig. 4*L′–N*). This suggests that after NMDA treatment the presumably unique membrane compartment in which PS1 resides is abnormally redistributed and enlarged in the core of NER.

Progressive changes in the ultrastructural morphology of NMDA-induced tubular structures

The altered intracellular membranes that initially appeared (E8–E10) in MNs after NMDA treatment showed a long-term evolution to autophagic-like structures. After E16, tubulovesicular structures progressively became more electrodense, and they started to be enfolded by new multiple membrane profiles that were more evident at older ages (E18) (Fig. 6*A*,*B*). Dense tubular structures were intermixed with a plethora of different sized vesicles and small vacuoles. All these structures form the core of the NER at these embryonic ages, being surrounded by Golgi profiles as in early stages. Rough ER was found at the most peripheral area of the perykaryon showing a normal appearance. On E20 and 21, the oldest ages studied, multilamellar structures were more pleomorphic and bizarre and arranged in the form of intricate membrane whorls. Moreover, autophagic bodies containing internalized portions of cytoplasm, mitochondria, and other organelles were frequently present at these stages (Fig. 6*C*). Although, multilamellated bodies and a redistribution of Golgi apparatus have also been described in the postaxotomy chromatolytic reaction (Barron et al., 1971), to our knowledge, the tubulovesicular structures described here have never been detected in axotomized MNs.

DISCUSSION

The results concerning the response of chick embryo spinal cord to exogenous NMDA confirm and extend our previous studies in which we reported that the vulnerability of MNs to develop acute excitototoxic necrosis can be transiently abolished by previous treatment with excitotoxins (Calderó et al., 1997; Lladó et al., 1999). When the regimen of chronic NMDA treatment for inducing tolerance to excitotoxins coincides with the major period for programmed cell death in chick embryo MNs (E5–E9), it was paradoxically observed that the NMDA treatment also results in a target-independent rescue of many MNs that otherwise would die (Lladó et al., 1999). However, the detailed structural studies presented here demonstrate that the MNs are rescued by NMDA at the expense of suffering conspicuous cytopathological alterations that are not obvious when examined with conventional light microscopy. Changes are found early during the period of treatment, and these persisted even after stopping NMDA administration. At earlier periods (E8–E10) the structural alterations are only seen in the electron microscope and consist of vacuolar transformation of the MN cytoplasm with accumulation of membrane bound tubulovesicular organelles, without any noticeable changes in the nucleus or mitochondria. This kind of damage does not greatly compromise neuronal survival after the main period of programmed MN death, because a large number of the altered MNs remain alive during for long period (at least until E20–E21, the last ages studied) (Lladó et al., 1999, their Fig. 2*A*). Similar cytoplasmic vacuolar alterations, although much more pronounced, are typical of NMDA-induced acute excitotoxic MN death, accompanied by severe nuclear and mitochondrial damage; however, tubulovesicular organelles do not occur in this case (Ciutat et al., 1996; Calderó et al., 1997). Therefore, it appears that, after chronic NMDA treatment, MNs become resistant to acute excitotoxic cell death, not as a consequence of survival-promoting trophic effects of NMDA, but because the induced changes are below the threshold for dying. Thus, MNs suffering this kind of excitotoxic injury would be incompetent to respond to the normal regulatory mechanisms necessary for the induction or execution of programmed cell death. Because it has been recently reported that apoptosis and excitotoxic necrosis are mutually exclusive (Lankiewicz et al., 2000), we are currently conducting experiments to specifically address this question in spinal cord MNs. Consistent with a modest excitotoxic response, we found that the mitochondria and nucleus, which are essential targets for mediating excitotoxic neuronal death (Ankarcrona et

Table 1. Mapping of Nissl-excluded area with distinct fluorescent markers in MNs of E16 NMDA-treated embryos

			Core	
	Outside	Border	Periphery	Inner
CGRP	+/−	+++	+	+
GS28	+/−	++	+	+
Membrin	+	+	++	++
WGA	+/−	+++	++	++
KDELr	+/−	++	−	−
Cystatin C	+/−	+/−	+++	+++
FM1-43 uptake	+	+	+++	+++
EAA1	++	++	++	++
Cholera toxin B uptake	+	+++	+	+
Rab11	+/−	+/−	++	++
APP	+/−	+/−	+	+
βAP	+/−	+/−	+	+
PS1	+/−	+/−	+++	+
Ubiquitin	+	+	+	+

Degree of immunoreactive signal (subjective scale): +/− traces, + weak, ++ medium, +++ strong.

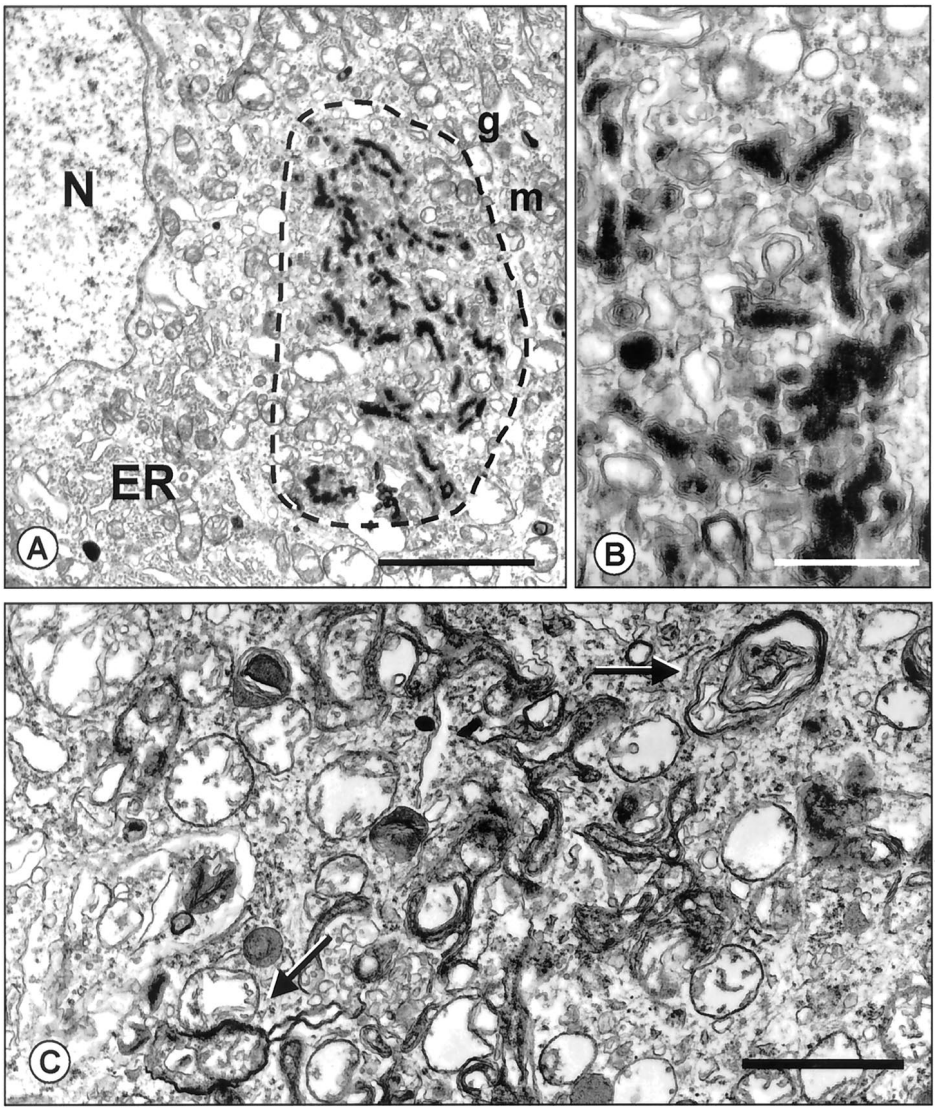

Figure 6. Ultrastructure of MN cytoplasm of E18 (*A, B*) and E20 (*C*) embryos previously treated with NMDA showing the evolution of tubulovesicular structures to autophagic-like vacuoles. *A,* By E18 tubulovesicular structures (delimited by *dashed lines*) become more electrodense, and they are enfolded by new membrane profiles, as seen in a high magnification in *B*; note the accumulation of vesicles intermixed with the electrodense structures. *C,* By E20 many multilamellar structures and autophagic bodies, some of them engulfing portions of cytoplasm and mitochondria (*arrows*), are present. *N,* Nucleus; *m,* mitochondrion; *ER,* endoplasmic reticulum. Scale bars: *A*, 3.60 μm; *B*, 0.90 μm; *C*, 1.80 μm.

al., 1995; Schinder et al., 1996; Pang and Gedds, 1997; Castilho et al., 1998), appear to be unaffected after chronic NMDA treatment. Because glutamate receptors are downregulated after chronic NMDA treatment (Lladó et al., 1999), the calcium entry elicited by NMDA may be decreased compared with the normal situation. This may protect mitochondria from the calcium overloading required to trigger NMDA receptor-stimulated neuronal death (Stout et al., 1998).

Another interesting aspect of our results is the relationship between the sublethal excitotoxic response and the slow developing pathogenic process in neurodegenerative diseases. It is interesting to note that whereas excitotoxicity seems to play an important role in the pathogenesis of Huntington's disease (HD), transgenic HD mice exhibit a resistance to NMDA receptor-mediated cell death (Hansson et al., 1999), similar to our model of sublethal excitotoxicity in MNs. Furthermore, in transgenic HD mice, degenerating neurons display vacuolar changes with organelle preservation (Turmaine et al., 2000), similar to those we found in MNs after chronic NMDA treatment. On the other hand, because slow excitotoxicity may also operate in experimental and human ALS, the present results may be relevant for understanding ALS pathogenesis.

One pathological feature in ALS that is considered to be an early event that precedes degeneration and loss of MNs, is the alteration of the Golgi apparatus (Gonatas et al., 1992). We show that abnormalities in the arrangement of Golgi apparatus and other components of the secretory–lysosomal pathway are conspicuous and long-lasting in MNs after chronic NMDA treatment, providing the first evidence that the endomembranous system is a major target for a sublethal excitotoxic injury. We cannot determine whether the primary site of damage is the intracellular membrane compartments or secondary to primary disturbance of cytoskeletal elements. It is well established that the dynamics and structural integrity of cytoskeleton and membrane organelles are both closely interdependent and calcium-regulated (Lippincott-Schwartz, 1998). Our data on silver staining and neurofilament immunolabeling indicates that a rearrangement of intracellular filaments surrounding NER, consistent with the newly established intracellular architecture, has occurred.

Although we have not been able to determine how the NMDA-induced redistribution of intracellular membrane compartments affects the processing, sorting, and targeting of specific molecules, it is clear that membrane trafficking is altered by NMDA treatment. However, the identity of the enlarged membrane compartment is difficult to examine to date, because of the fact that most of the molecular reagents available for membrane traffic studies

do not work in avian tissues. Another problem impeding further biochemical studies is the difficulty in using cultured MNs for these studies. Cultured chick MNs do not survive long enough *in vitro* for the chronic studies with NMDA that are required to examine the sublethal changes observed *in vivo*.

Nonetheless, based on the intracellular redistribution of CGRP and KDELr we observe on E16, it seems clear that the intricate membranous structures inside NER are *trans* oriented with respect to the Golgi. Thus, it is seems likely that the enlarged tubulovesicular membranes belong to the *trans*-Golgi network, a region in which secretory cargo is sorted and packaged into post-Golgi carriers that move and fuse with the cell surface (Lippincott-Schwartz et al., 2000). In neurons, the *trans*-Golgi network is a central part of polarized membrane protein trafficking and sorting used for specific targeting to dendrites or axons (Trimmer, 1999). Multiple pathways intersect and exchange components in the vacuolar system in a highly dynamic way, and an imbalance between the amount of membrane addition and loss may introduce marked changes in the size and identity of individual compartments. The accumulation of PS in the NER we observe may be a consequence of altered trafficking, because it is thought that PSs reside mainly in specific domains of the ER and pre-Golgi membranes (Lah et al., 1997; Kim et al., 2000). The same situation may account for the accumulation of APP and βAP.

The *trans*-Golgi network is known to interact with the recycling endosomal system. Our observation of a late accumulation of FM1-43 within vesicles in the NER is consistent with this interpretation, because it has been shown that this marker accumulates in TGN after endocytosis in hippocampal neurons (Maletic-Savatic and Malinow, 1998).

The moderate increase in Rab11, a product known to be highly concentrated in the pericentriolar recycling compartment Ullrich et al., 1996; Johannes et al., 2000), also suggests that post-Golgi and late endocytic membrane vesicles converge in the NER, similar to the TGN. By contrast, early endosomes do not accumulate inside this region, as demonstrated by the widespread distribution of EEA1 immunolabeling in soma and dendrites of both normal and NMDA-treated MNs. This is consistent with other evidence concerning endocytic pathways in neurons (Mundigl et al., 1993; Wilson et al., 2000). Because we have not detected any accumulation of axonally transported CTB inside the NER, it is probable that the endosomal organelles are derived from dendrites not from axons. It is known that endocytic organelles from dendrites and axons follow separate pathways (Mundigl et al., 1993). In agreement with studies on cholera toxin uptake dynamics in non-neural cells (Majoul et al., 1996), we have observed an accumulation of internalized CTB in Golgi and small particles, which presumably are lysosomes. Similar observations were reported in chick embryo MNs after axonal transport of horseradish peroxidase (Chu-Wang and Oppenheim, 1980).

Although MNs that undergo the NMDA-induced changes described here are viable, it seems likely that they may die later or that they are more susceptible to later injury. In fact, these MNs progressively acquire an ultrastructural morphology commonly found in degenerating neurons, including autophagosomes and pleomorphic inclusion bodies. Endocytosis and autophagy are common events in some types of naturally occurring neuronal death (Hornung et al., 1989), and it was recently found that they occur during caspase-independent neuronal death (Xue et al., 1999; Oppenheim et al., 2001; Yaginuma et al., 2001). It is also interesting that in HD brain the aberrant accumulation of huntingtin seems to induce neuronal death because of alterations in the endosomal–lysosomal–vacuolar pathway (Kegel et al., 2000). A wide variety of cytoplasmic inclusions indicative of alterations of the vacuolar system are also commonly found in MNs from human ALS patients (Chou, 1995). One inclusion, the so-called Bunina body (BB), is considered to be a specific marker of the disease. BBs are formed by amorphous material surrounded by vesicles and tubular structures (Sasaki and Maruyama, 1993) and appear to be a special type of autophagic vacuole (Hart et al., 1977). Tubulovesicular structures associated with BBs are selectively immunostained by antibodies against cystatin C, and it has been proposed that they represent an abnormal accumulation of unknown proteinaceus material associated with the Golgi apparatus (Okamoto et al., 1993). The fact that we detected an accumulation of cystatin C inside the NER suggests that this may reflect an early stage in generation of BBs.

In conclusion, the sublethal ultrastructural and other changes we observe in spinal MNs after chronic NMDA treatment are similar to the abnormalities observed in certain pathological conditions such as HD and ALS. For this reason this NMDA model may be useful for preclinical studies of potential treatment strategies.

REFERENCES

Agrawal SK, Fehlings MG (1997) Role of NMDA and non-NMDA ionotropic glutamate receptor in traumatic spinal cord axonal injury. J Neurosci 17:1055–1063.

Ankarcrona M, Dypbukt JM, Bonfoco E, Zhivotovsky B, Orrenius S, Lipton SA, Nicotera P (1995) Glutamate-induced neuronal death: a succession of necrosis or apoptosis depending on mitochondrial function. Neuron 15:961–973.

Barron KD, Chiang TY, Daniels AC, Doolin PF (1971) Subcellular accompaniments of axon reaction in cervical motoneurons of the cat. Prog Neuropathol 1:255–280.

Calderó J, Casanovas A, Sorribas A, Esquerda JE (1992) Calcitonin gene-related peptide in rat spinal cord motoneurons: subcellular distribution and changes induced by axotomy. Neuroscience 48:449–461.

Calderó J, Ciutat D, Lladó J, Castán E, Oppenheim RW, Esquerda JE (1997) Effects of excitatory amino acids on neuromuscular development in chick embryo. J Comp Neurol 387:73–95.

Castilho RF, Hansson O, Ward MW, Budd SL, Nicholls DG (1998) Mitochondrial control of acute glutamate excitotoxicity in cultured cerebellar granule cells. J Neurosci 18:10277–10286.

Chou SM (1995) Pathology of motor system disorder. In: Motor neuron disease (Leigh PN, Swash M eds), pp 53–92. London: Springer.

Chu-Wang I-W, Oppenheim RW (1980) Uptake, intra-axonal transport and fate of horseradish peroxidase in embryonic spinal neurons of the chick. J Comp Neurol 193:753–776.

Ciutat D, Calderó J, Oppenheim RW, Esquerda JE (1996) Schwann cell apoptosis during normal development and after axonal degeneration induced by neurotoxins in the chick embryo. J Neurosci 16:3979–3990.

Gonatas NK, Stieber A, Mourelatos Z, Chen Y, Gonatas JO, Appel SH, Hays AP, Hickey WF, Hauw JJ (1992) Fragmentation of the Golgi apparatus of motor neurons in amyotrophic lateral sclerosis. Am J Pathol 140:731–737.

Griffiths G, Ericsson M, Krijnse-Locker J, Nilsson T, Goud B, Söling HD, Tang BL, Wong SH, Hong W (1994) Localization of the Lys, Asp, Glu, Leu, tetrapeptide receptor to the Golgi complex and the intermediate compartment in mammalian cells. J Cell Biol 127:1557–1574.

Hamburger V, Hamilton HL (1951) A series of normal stages in the development of the chick embryo. J Morphol 88:49–92.

Hansson O, Petersén Å, Leist M, Nicotera P, Castilho RF, Brundin P (1999) Transgenic mice expressing a Huntington's disease mutation are resistant to quinolinic acid-induced striatal excitotoxicity. Proc Natl Acad Sci USA 96:8727–8732.

Hart MN, Cancilla PA, Frommes S, Hirano A (1977) Anterior horn cell degeneration and Bunina-type inclusions associate with dementia. Acta Neuropathol 38:225–228.

Hornung JP, Koppel H, Clarke PGH (1989) Endocytosis and autophagy in dying neurons: an ultrastructural study in chick embryos. J Comp Neurol 283:425–437.

Johannes WM, Galli T, Mayau V, Goud B, Salamero J (2000) Rab11 regulates the compartmentalization of early endosomes required for efficient transport from early endosomes and trans-Golgi network. J Cell Biol 151:1207–1220.

Kegel KB, Kim, Sapp E, Mcintyre C, Castaño JG, Aronin N, DiFiglia M

(2000) Huntingtin expression stimulates endosomal.lysosomal activity, endosome tubulation and autophagy. J Neurosci 20:7268–7278.
Kim SH, Lah JJ, Thinakaran G, Levey A, Sisodia SS (2000) Subcellular localization of presenilins: association with unique membrane pool in cultured cells. Neurobiol Dis 7:99–117.
Klausner RD, Donaldson JG, Lippincott-Schwartz J (1992) Brefeldin A: insights into the control of membrane traffic and organelle structure. J Cell Biol 5:1071–1080.
Lah JJ, Heilman CJ, Nash NR, Rees HD, Yi H, Counts SE, Levey AI (1997) Light and electron microscopy localization of presenilin-1 in primate brain. J Neurosci 17:1971–1980.
Lankiewicz S, Luetjens CM, Bui NT, Krohn AJ, Poppe M, Cole GM, Saido TC, Prehn JHM (2000) Activation of calpain I converts excitotoxic neuron death into a caspase-independent cell death. J Biol Chem 275:17064–17071.
Ledger PW, Tanzer ML (1984) Monensin-a perturbant of cellular physiology. Trends Biochem Sci 9:313–314.
Lewis MJ, Pelham RB (1992) Ligand-induced redistribution of a human KDEL-receptor from the Golgi complex to the endoplasmic reticulum. Cell 68:353–364.
Lewis PR (1977) Metal precipitation methods for hydrolitic enzymes. In: Practical methods in electron microscopy (Glauert AM, ed), Vol 5, Part I, Staining methods for sectioned material staining (Lewis PR, Knight DP, eds), pp 137–223. Amsterdam: North-Holland.
Lieberman AR (1971) The axon reaction: a review of the principal features of perikaryal responses to axon injury. Int Rev Neurobiol 14:49–124.
Lippincott-Schwartz J (1998) Cytoskeletal proteins and Golgi dynamics. Curr Opin Cell Biol 10:52–59.
Lippincott-Schwartz J, Yuan LC, Tipper C, Klausner RD (1991) Brefeldin A's effects on endosomes, lysosomes and TGN suggest a general mechanism for regulating organelle structure and membrane trafficking. Cell 67:601–616.
Lippincott-Schwartz J, Roberts TH, Hirschberg K (2000) Secretory protein trafficking and organelle dynamics in living cells. Annu Rev Cell Dev Biol 16:557–589.
Lladó J, Calderó J, Ribera J, Tarabal O, Oppenheim RW, Esquerda JE (1999) Opposing effects of excitatory amino acids on chick embryo spinal cord motoneurons: excitotoxic degeneration or prevention of programmed cell death. J Neurosci 19:10803–10812.
Majoul V, Bastiaens PIH, Söling HD (1996) Transport of an external Lys-Asp-Glu-Leu (KDEL) protein from the plasma membrane to the endoplasmic reticulum: studies with cholera toxin in Vero cells. J Cell Biol 133:777–789.
Maletic-Savatic M, Malinow R (1998) Calcium-evoked dendritic exocytosis in cultured hippocampal neurons. Part 1: trans-Golgi network-derived organelles undergo regulated exocytosis. J Neurosci 18:6803–6813.
Mellman I, Simons K (1992) The Golgi complex: In vitro veritas? Cell 68:829–840.
Migheli A, Atzori C, Piva R, Tortarolo M, Girelli M, Sciffer D, Bendotti C (1999) Lacks of apoptosis in mice with ALS. Nat Med 5:966–967.
Mourelatos Z, Gonatas NK, Stieber A, Gurney ME, Dal Canto MC (1996) The Golgi apparatus of spinal cord motor neurons in transgenic mice expressing mutant Cu,Zn superoxide dismutase becomes fragmented in early, preclinical stages of the disease. Proc Natl Acad Sci USA 93:5472–5477.
Mundigl O, Matteoli M, Daniell L, Thomas-Reetz A, Metcalf A, Jahn R, De Camilli P (1993) Synaptic vesicle proteins and early endosomes in cultured hippocampal neurons: differential effects of Brefeldin A in axon and dendrites. J Cell Biol 122:1207–1221.
Nambiar MP, Oda T, Chen C, Kuwazuru Y, Wu HC (1993) Involvement of the Golgi region in the intracellular trafficking of cholera toxin. J Cell Physiol 154:222–228.
Novikoff AB, Goldfischer S (1961) Nucleosidediphosphatase activity in the Golgi apparatus and its usefulness for cytological studies. Proc Natl Acad Sci USA 47:802.
Okamoto K, Hirai S, Amari M, Watanabe M, Sakurai A (1993) Bonina bodies in amyotrophic lateral sclerosis immunostained with rabbit anti-cystatin C serum. Neurosci Lett 162:125–128.
Oppenheim RW, Flavell RA, Vinsant S, Prevette D, Kuan C, Rakic P (2001) Programmed cell death of developing mammalian neurons after genetic deletion of caspases. J Neurosci 21:4752–4760.
Orci L, Perrelet A, Ravazzola M, Wieland F, Schekmman R, Rothman JE (1993) "BFA bodies": a subcompartment of the endoplasmic reticulum. Proc Natl Acad Sci USA 90:11089–11093.
Pang Z, Gedds JW (1997) Mechanisms of cell death induced by the mitochondrial toxin 3-nitropropionic acid: acute excitotoxic necrosis and delayed apoptosis. J Neurosci 17:3064–3073.
Pena E, Berciano MT, Fernández R, Ojeda JL, Lafarga M (2001) Neuronal body size correlates with the number of nucleoli and Cajal bodies, with the organization of the splicing machinery in rat trigeminal ganglion neurons. J Comp Neurol 430:250–263.
Rothstein JD (1996) Excitotoxicity hypothesis. Neurology 47:S19–S26.
Sasaki S, Maruyama S (1993) Ultrastructural study of Bunina bodies in the anterior horn neurons of patients with amyotrophic lateral sclerosis. Neurosci Lett 154:117–120.
Schinder AF, Olson EC, Spitzer NC, Montal M (1996) Mitochondrial dysfunction is a primary event in glutamate neurotoxicity. J Neurosci 16:6125–6133.
Stout AK, Raphael HM, Kanterewicz BI, Klann E, Reynolds IJ (1998) Glutamate-induced neuron death requires mitochondrial calcium uptake. Nat Neurosci 1:366–373.
Subramaniam VN, Peter F, Philp R, Wong SH, Hong W (1996) GS28 a 28-kilodalton Golgi SNARE that participates in ER-Golgi transport. Science 272:1161–1163.
Trimmer JS (1999) Sorting out receptor trafficking. Neuron 22:411–417.
Turmaine M, Raza A, Mahal A, Mangiarini L, Bates GP, Davies SW (2000) Nonapoptotic neurodegeneration in a transgenic mouse model of Huntington's disease. Proc Natl Acad Sci USA 97:8093–8097.
Ullrich O, Reinsch S, Urbe S, Zerial M, Parton RG (1996) Rab1 regulates recycling through the pericentriolar recycling endosome. J Cell Biol 135:913–924.
Wilson JM, de Hoop M, Zorzi N, Toh B-H, Dotti CG, Parton RG (2000) EEA1, a tethering protein of the early sorting endosome, shows a polarized distribution in hippocampal neurons, epithelial cells, and fibroblasts. Mol Biol Cell 11:2657–2671.
Wrathall JR, Choiniere D, Teng YD (1994) Dose-dependent reduction of tissue loss and junctional impairment after spinal cord trauma with the AMPA/kainate antagonist NBQX. J Neurosci 14:6598–6607.
Xue L, Fletcher GC, Tolkovsky AM (1999) Autophagy is activated by apoptotic signaling in sympathetic neurons: an alternative mechanism of death execution. Mol Cell Neurosci 14:180–198.
Yaginuma A, Shiraiwa N, Shimada T, Nishiyama K, Hong J, Wang S, Momoi T, Uchiyama Y, Oppenheim RW (2001) Caspase activity is involved in but is dispensable for early motoneuron death in the chick embryo spinal cord. Mol Cell Neurosci 18:168–182.